

But we have

$$\hat{n}_\Lambda(\text{c.m.}) \equiv (\hat{\pi} \times \hat{\Lambda}) / |\hat{\pi} \times \hat{\Lambda}| = (\hat{\pi} \times \hat{\Lambda}) / \sin\theta_\Lambda \quad (\text{A12})$$

and

$$p_\Sigma(\text{c.m.}) = p_\Sigma(\text{c.m.})\hat{z}. \quad (\text{A13})$$

We also have (see Fig. 3)

$$\hat{\pi} = \hat{z} \cos\theta_\Sigma + \hat{y} \sin\theta_\Sigma, \quad (\text{A14})$$

and

$$\hat{\Lambda} = \hat{z} \cos\alpha + \sin\alpha(\hat{x} \cos\phi + \hat{y} \sin\phi), \quad (\text{A15})$$

so that

$$\hat{z} \cdot (\hat{\pi} \times \hat{\Lambda}) = -\sin\theta_\Sigma \sin\alpha \cos\phi. \quad (\text{A16})$$

Combining Eqs. (A10) through (A16) we obtain

$$\hat{q} \cdot \hat{n}_\Lambda = [p_\Sigma(\text{c.m.}) \sin\alpha / p_\Sigma(\Lambda)] \cos\phi \sin\theta_\Sigma / \sin\theta_\Lambda. \quad (\text{A17})$$

The expression in square brackets involves quantities known or measurable for each event. It is equal to $\sin\beta$,

as follows from the Lorentz invariance of the transverse momentum components of p_Σ in the transformation from the c.m. to Λ frame:

$$p_\Sigma(\text{c.m.}) \sin\alpha = p_\Sigma(\Lambda) \sin\beta. \quad (\text{A18})$$

Combining Eqs. (A17) and (A18) we obtain Eq. (A8), i.e., Eq. (49). Also we see from Eq. (A18) that the angle β also depends (through α) only on the angle γ , constants of nature, and the beam momentum, and is consequently measurable for each event. (Note that the Euclidean relation that seems implied in Fig. 3, namely $\beta = \gamma - \alpha$, is not valid due to its non-Lorentz-invariant nature.)

Lastly, we derive Eq. (56). By definition $\cos\theta_\Lambda = \hat{\pi}(\text{c.m.}) \cdot \hat{\Lambda}(\text{c.m.})$. Then Eqs. (A14) and (A15) give

$$\hat{\pi} \cdot \hat{\Lambda} = \cos\alpha \cos\theta_\Sigma + \sin\alpha \sin\theta_\Sigma \sin\phi, \quad (\text{A19})$$

which is Eq. (56).

Reactions $K^- p \rightarrow \text{Hyperon} + \text{Meson}$ at 3.5 GeV/c

BIRMINGHAM-GLASGOW-LONDON (I.C.)-OXFORD-RUTHERFORD COLLABORATION*

(Received 4 April 1966)

A study has been made of some of the quasi-two-body final states (in which one of the particles is a hyperon) produced by 3.5-GeV/c K^- mesons on protons. The analysis has been performed with 310 000 photographs taken in the 81-cm Saclay hydrogen bubble chamber. The cross sections for most of the reactions are lower than have been observed at lower incident momenta. Many of the reactions are characterized by a forward peaking of the production angular distribution of the final-state meson, but in a few cases a significant backward peak has been observed. Decay distributions of unstable particles have been investigated to obtain more information about the production processes. The $Y_1^{*+}(1385)$ decay is consistent with the $Y^*\pi^-$ final state being produced by K^* exchange, but in the case of the production of vector mesons, it is difficult to draw any conclusion concerning the spin of the exchanged particle. An enhancement was observed at 1645 MeV in the $\Sigma^+\pi^+$ system. It is difficult to interpret this in terms of the decay of the neutral $Y_1^*(1660)$.

1. INTRODUCTION

DESPITE intensive theoretical and experimental studies, the subject of the production mechanism of elementary-particle reactions at medium and high

energies is still far from being completely understood. It is clear that experimental data are required for a large number of different reactions over a wide range of incident energies, and with high statistical accuracy. In this article we describe some of the features of the interactions of 3.5-GeV/c K^- mesons with protons.

Some results of this experiment have already been published in two articles; one¹ on the discovery of the $K^*(1400)$ and the other² on a determination of the parity of the $Y^*(1660)$. In this paper we present results on two-body channels involving a strange baryon. An

* Members of the collaboration are:

M. Haque and B. Musgrave, Department of Physics, University of Birmingham, Birmingham, England.

W. M. R. Blair and A. L. Grant (present address: CERN, Geneva, Switzerland); I. S. Hughes, P. J. Negus, and R. M. Turnbull, Department of Natural Philosophy, University of Glasgow, Glasgow, Scotland.

A. A. Z. Ahmad (present address: Atomic Energy Commission, Lahore, Pakistan); S. Baker, L. Celnikier (present address: CERN, Geneva, Switzerland); S. Misbahuddin (present address: Atomic Energy Commission, Lahore, Pakistan) and I. O. Skillicorn (present address: Brookhaven National Laboratory, Upton, New York) Department of Physics, Imperial College, London, England.

A. R. Atherton, A. D. Brody, G. B. Chadwick (present address: Stanford Linear Accelerator Center, Stanford, California); W. T. Davies, J. H. Field (present address: University of California, La Jolla, California); P. M. D. Gray, D. E. Lawrence, J. G. Loken (present address: Argonne National Laboratory, Argonne, Illi-

nois); L. Lyons, J. H. Mulvey, A. J. Oxley, and C. A. Wilkinson, Department of Nuclear Physics, University of Oxford, Oxford, England.

C. M. Fisher, E. Pickup, L. K. Rangan, J. M. Scarr (present address: Brookhaven National Laboratory, Upton, New York), and A. M. Segar, Rutherford High-Energy Laboratory, Chilton, Berkshire, England.

¹ M. Haque *et al.*, Phys. Letters 14, 338 (1965).

² A. Leveque *et al.*, Phys. Letters 18, 69 (1965).

analysis of those interactions producing K mesons and nonstrange baryons will be published separately.³

The data presented in this paper were obtained from hydrogen-bubble-chamber exposures carried out in the $M2$ beam⁴ at CERN in 1963. A total of 310 000 photographs of 3.5-GeV/c K^- mesons was obtained from the 81-cm Saclay hydrogen bubble chamber.

2. EXPERIMENTAL PROCEDURE

The film was scanned twice for events with a visible strange-particle decay, and a comparison between the two scans was made to calculate the efficiency. In addition to interactions, τ decays were recorded. The constitution of the beam was thus determined to be $(63 \pm 4)\%$ K 's, $(24 \pm 5)\%$ π 's, and $(13 \pm 5)\%$ μ 's.

The Rutherford Laboratory bubble-chamber analysis system⁵ was used for the geometrical reconstruction and kinematical fitting of events, and for calculating and plotting quantities of physical interest.

Separation into final states was made on the basis of the χ^2 probabilities of the multivertex fits to events for the various possible hypotheses. An event was assigned to a particular hypothesis A if the χ^2 probability $P_{\chi^2}(A)$ for the hypothesis satisfied the criteria:

$$P_{\chi^2}(A) > 0.05,$$

$$P_{\chi^2}(A) > 5P_{\chi^2}(X),$$

where X refers to any other possible hypotheses for the event. In calculating cross sections, events which were ambiguous as to two hypotheses were assigned to these hypotheses in the ratio of the numbers of nonambiguous fits. A discussion of the purity of the selected samples is given in Appendix B.

Corrections for unseen decay modes of the Λ and K^0 were made assuming the $\Delta I = \frac{1}{2}$ rule for these decays. A further correction factor was calculated to allow for undetected charged decays of Λ 's and Σ 's. A more detailed description of these weighting factors may be found in Appendix A, or in Ref. 6.

Cross sections of resonant intermediate states have been estimated using a maximum-likelihood program, which fitted Breit-Wigner curves plus phase-space background to all the resonant channels for a particular final state and so takes into account reflections of resonant peaks in other mass distributions of the same final state.

A maximum-likelihood method was also used to determine the values of density-matrix elements from the observed decay distributions of resonances. The

values expected according to the absorption model⁷ for these density-matrix elements have been calculated for the case of the production of vector mesons by K exchange. The values γ_1 and C_1 ⁷ were chosen as 0.042 and 0.64, respectively, to be consistent with the K^-p elastic-scattering data⁸ at 3.5 GeV/c; γ_2 was taken as $\frac{3}{4}\gamma_1$ and C_2 was set equal to unity. The production angular distributions for some of the reactions showing a forward peaking of the outgoing meson have been fitted by the formula

$$d\sigma/dt = Ke^{At},$$

where t is the momentum transfer. This has been done merely to obtain a convenient parametrization of the forward peak, and not because we believe there is any basic significance in the above formula. Values of A are given in Table IV at the end of this paper. Also shown there are the values of $|t-t_0|_{\max}$ up to which the fit was performed; t_0 is the momentum transfer in the extreme forward direction.

3. TWO-BODY FINAL STATES

As has been observed in other experiments⁸ in the few-GeV/c region with π or K beams, a significant contribution to the total cross section is made by quasi-two-body final states. In this section, results on some of the more important of these channels are discussed.

A. $K^-p \rightarrow \Lambda\pi^0$

The cross section for the $\Lambda\pi^0$ final state was found to be (115 ± 40) μb . Contamination from two-pion production was estimated from a consideration of the missing mass distribution obtained by deleting the charged tracks from $\Lambda\pi^+\pi^-$ events; it was found to be negligible. This was confirmed by examining the distribution of the square of the missing mass recoiling from the Λ , from events of the topology zero-prong $+\Lambda^0$ (see Fig. 1(a)). However, assuming the $\Sigma^+\pi^-$ and $\Sigma^0\pi^0$ final states to be produced by the exchange of a K^* of isospin $\frac{1}{2}$, we estimate the $\Sigma^0\pi^0$ contamination in this channel to be 2.5 ± 0.2 events. The value of the cross section has been corrected for these $\Sigma^0\pi^0$ events.

The production angular distribution for the $\Lambda\pi^0$ events is shown in Fig. 1(b). This channel, in common with many others, exhibits low-momentum transfer to the baryon, expected on the one-meson-exchange production model, as well as the sharp collimation of the distribution associated with absorption effects.

³ M. Haque *et al.* (unpublished report). A more detailed account of the elastic-scattering reaction has been given by J. D. Gordon, *Phys. Letters* 21, 117 (1966).

⁴ J. Goldberg and J. M. Perreau, CERN Report 63-12 (unpublished).

⁵ J. W. Burren, J. M. Scarr, E. C. Sedman, J. Sparrow, and A. J. Wilson, Rutherford Laboratory Internal Reports (unpublished).

⁶ J. G. Loken, Ph.D. thesis, Oxford (unpublished).

⁷ J. D. Jackson, *Rev. Mod. Phys.* 37, 484 (1965), from which previous references to papers on the absorption model may be obtained.

⁸ See, for example, R. George *et al.*, in *Proceedings of the Oxford International Conference on Elementary Particles, 1965* (Rutherford High Energy Laboratory, Harwell, England, 1966), supplement, p. 69; Aachen-Berlin-CERN-London-Vienna Collaboration, *ibid.*, p. 71; and M. Deutschmann *et al.*, *Phys. Letters* 19, 608 (1965).

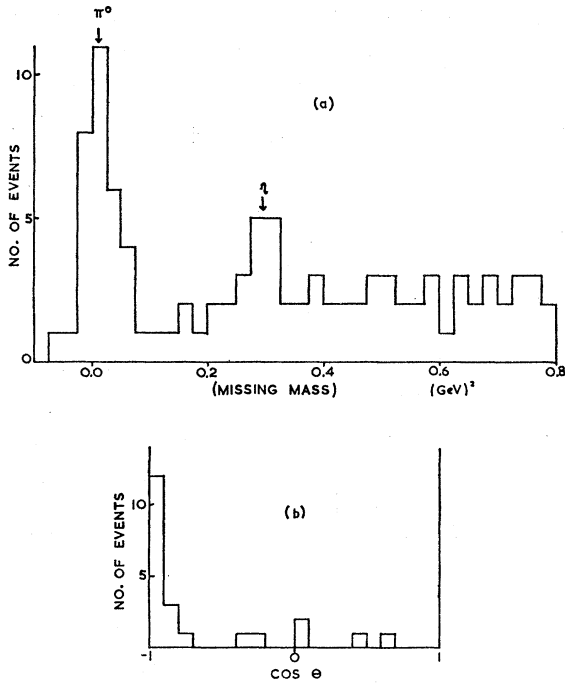


FIG. 1. (a) Histogram of the number of events plotted against the square of the missing mass from the Λ^0 from events of the topology zero-prongs $+\Lambda^0$. (b) Center-of-mass production angular distribution for the $\Lambda\pi^0$ final state. The figure contains 22 events. As with all production angular distributions in this article, θ is defined as the angle between the incident K^- meson and the final-state baryon. Thus meson exchange produces a peak at the left-hand side of the histogram, and baryon exchange would give rise to a peak on the right.

B. $K^-p \rightarrow \Sigma^+\pi^-$ and $\Sigma^-\pi^+$

The cross sections for the reactions $K^-p \rightarrow \Sigma^+\pi^-$ and $\Sigma^-\pi^+$ are (140 ± 10) and $(11 \pm 3) \mu\text{b}$, respectively. The $\Sigma^+\pi^-$ final state is almost entirely peripherally produced, as can be seen from the production angular distribution of Fig. 2. Also shown in this figure are the 12 events identified as $\Sigma^-\pi^+$, which in contrast have the baryon mainly in the forward hemisphere. This feature of a forward peaking of the baryon is common to many reactions at high energies,⁹ being especially noticeable in those cases for which meson exchange cannot take place. On the other hand, below about 2 GeV/c, the $\Sigma^-\pi^+$ production angular distribution, like those of several other K^-p final states,⁹ seems to be dominated more by S -channel effects than by the nature of the particles whose exchange is allowed.

C. $K^-p \rightarrow Y_1^{*+} (1385) \pi^-$

Figures 3(a), 3(b), and 3(c) show the $\Lambda\pi^+$, $\Lambda\pi^-$, and $\pi^+\pi^-$ effective-mass distributions (weighted against losses of charged decays) for 231 events assigned to the $\Lambda\pi^+\pi^-$ final state. The curves shown in Figs. 3(a) and 3(b) are phase-space curves renormalized to exclude the

⁹ A compilation of some of the experimental data has been given by L. Lyons, *Nuovo Cimento* 43, 888 (1966).

Y_1^{*+} peak. The cross-hatched distribution in Fig. 3(c) contains only those events outside the Y_1^{*+} region defined by the range of effective mass 1.34 to 1.41 GeV. A Breit-Wigner-plus-phase-space fit yielded the following results¹⁰ for the Y_1^* : $M = (1383 \pm 2)$ MeV; $\Gamma = (25 \pm 6)$ MeV; $Y_1^{*+}/(Y_1^{*+} + \text{phase space}) = (27 \pm 4)\%$. This corresponds to a cross section of $90 \pm 15 \mu\text{b}$ for the $Y_1^{*+}\pi^-$ channel.

Figure 4 shows the Dalitz plot for the $\Lambda\pi^+\pi^-$ final state. In addition to $Y_1^{*+}\pi^-$, there is some evidence for the channels $\Lambda\rho^0$ and Λf_0 . In choosing the sample of Y_1^{*+} events, no attempt was made to exclude events in the crossover regions of the ρ^0 and f_0 bands (indicated by the bands in Fig. 4) with the Y_1^{*+} band. There is no evidence for any strong interference effects in the Dalitz plot, and removing events in the overlap regions would result in considerable biasing of the Y_1^{*+} decay distribution.

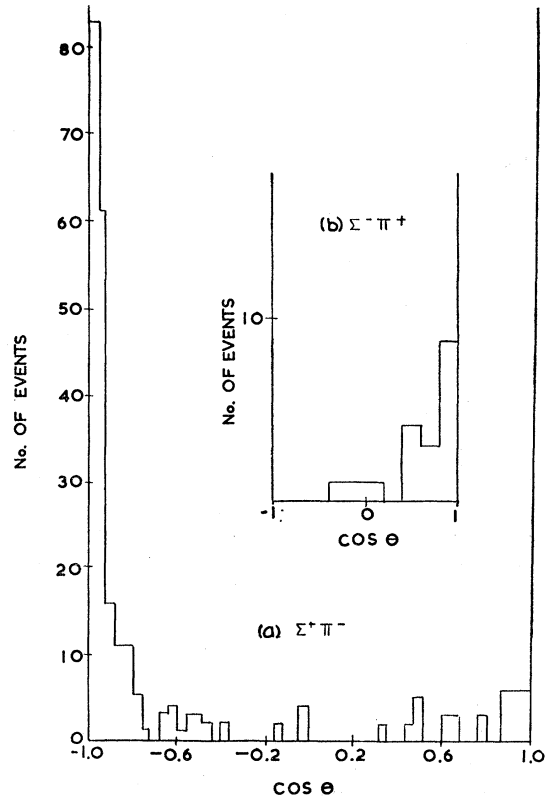


FIG. 2. Center-of-mass production angular distribution for the $\Sigma^\pm\pi^\mp$ final states. The 152 $\Sigma^+\pi^-$ events have a mean-weighting factor of 1.63, and the 12 $\Sigma^-\pi^+$ events are weighted by a factor whose average value is 1.58. The $\Sigma^-\pi^+$ angular distribution is typical of those for final states for which meson exchange cannot occur.

¹⁰ The width of ~ 20 MeV found for the $Y^*(1385)$ in this experiment after folding out the experimental resolution is less than the currently accepted (see Ref. 15) value of 44 MeV, based mainly on lower energy K^-p experiments, although R. Armenteros *et al.*, *Phys. Letters* 19, 75 (1965) recently also obtained a narrower value of (35 ± 3) MeV. The effect of decreasing Y_1^* width at higher energies in production experiments has been remarked on by R. K. Adair, *Rev. Mod. Phys.* 37, 473 (1965).

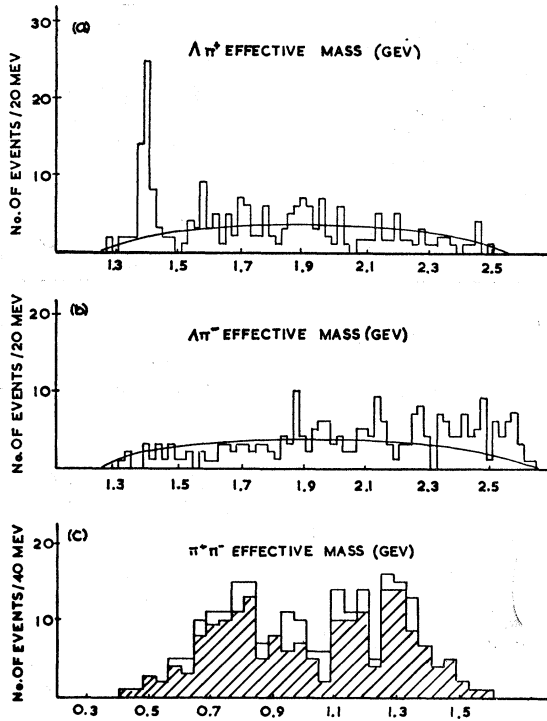


FIG. 3. The effective-mass distributions for (a) $\Lambda\pi^+$, (b) $\Lambda\pi^-$, and (c) $\pi^+\pi^-$ combinations from 231 events of the $\Lambda\pi^+\pi^-$ final state. The phase space curves for (a) and (b) are normalized to the region outside the $Y^*(1385)$. The cross-hatched distribution in (c) has had events in the $Y^*(1385)$ (defined by the $\Lambda\pi^+$ mass being between 1.34 and 1.41 GeV) removed.

The production angular distribution of the Y_1^* is backward-peaked (see Fig. 5). This, together with the absence of the negative charge state of the Y_1^* , indicates possible dominance of a single-particle-exchange

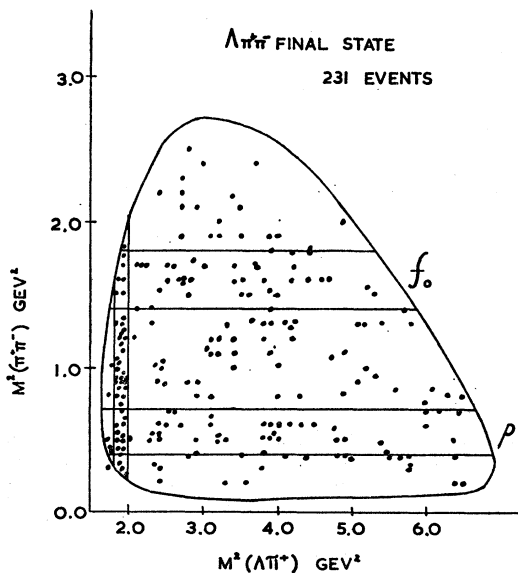


FIG. 4. Dalitz plot for the $\Lambda\pi^+\pi^-$ final state. The bands show the positions of the Y^* , ρ^0 , and f_0 .

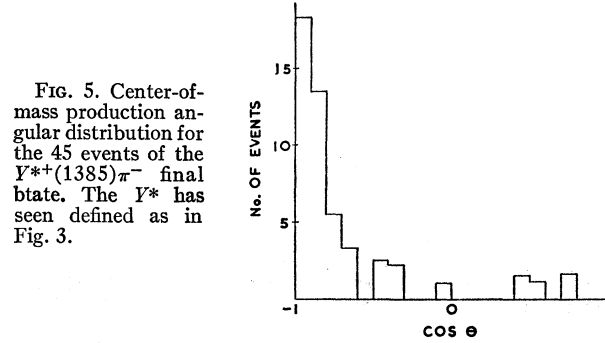


FIG. 5. Center-of-mass production angular distribution for the 45 events of the $Y^*(1385)\pi^-$ final state. The Y^* has been defined as in Fig. 3.

amplitude in the production. Only the exchange of K^* 's is possible since, as in all two-body reactions including a pion in the final state, pseudoscalar (K) exchange is forbidden by spin and parity conservation at the meson vertex.

The decay of the $Y^*(1385)$ can be described in terms of density-matrix elements by the formula¹¹

$$W(\theta, \phi) = (3/4\pi) [\rho_{33} \sin^2\theta + \rho_{11} (\frac{1}{3} + \cos^2\theta) - \frac{2}{3}\sqrt{3} \operatorname{Re}\rho_{3,-1} \sin^2\theta \cos 2\phi - \frac{2}{3}\sqrt{3} \operatorname{Re}\rho_{31} \sin 2\theta \cos\phi].$$

According to the Stodolsky-Sakurai¹² model for $Y^*(1385)$ production by the exchange of the $K^*(890)$, the density-matrix elements should have the values given in Table I. The experimental values are seen to be in satisfactory agreement with the prediction, implying that the possible admixture of $E2$ and $L2$ amplitudes with the dominant $M1$ one is probably small.

Figure 6 shows the experimental decay distributions with respect to axes defined in the figure caption, together with the best fit of the general formula for Y^*

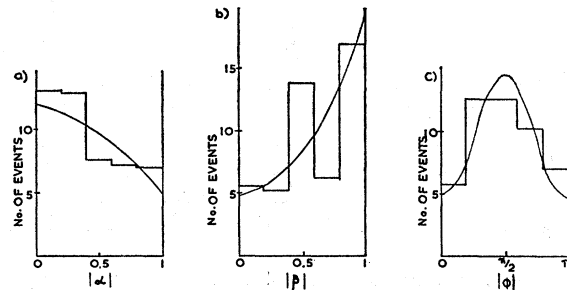


FIG. 6. Decay distributions for the $Y^*(1385)\pi^-$ events. The curves, which are shown only to give an indication of the quality of the fit, are the projections of the general decay distribution with the values of the density-matrix elements given in Table I. The angles are defined as follows. Let $\hat{\pi}^+$ denote a unit vector in the direction of the π^+ in the Y_1^* rest frame, \hat{p} denote the corresponding vector for the target proton, and \mathbf{n} be the normal to the Y_1^* production plane. Then the three direction cosines α , β , γ are $\alpha = \hat{\pi}^+ \cdot \hat{p}$, $\beta = \hat{\pi}^+ \cdot \mathbf{n}$, $\gamma = \hat{\pi}^+ \cdot (\hat{p} \times \mathbf{n})$. The angle ϕ (Treiman-Yang angle) between the normals to the production and decay planes of the Y_1^* is defined by $\tan\phi = \beta/\gamma$. For a given event, only two of the three angles plotted are independent.

¹¹ The angle ϕ is the Treiman-Yang angle defined in Fig. 6, and $\cos\theta$ in the formula is the same as α in the figure.

¹² L. Stodolsky and J. J. Sakurai, Phys. Rev. Letters 11, 90 (1963); L. Stodolsky, Phys. Rev. 134, B1099 (1964).

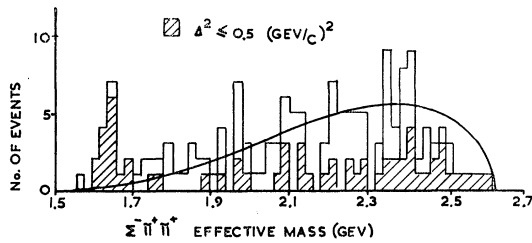


FIG. 7. The $\Sigma^-\pi^+\pi^+$ effective-mass distribution (unweighted) for 165 events in the $\Sigma^-\pi^+\pi^+\pi^-$ final state. The shaded distribution contains events with momentum transfer to the $\Sigma^-\pi^+\pi^+$ combination less than 500 $(\text{MeV}/c)^2$. Especially when this selection is made, the $Y^*(1660)$ is clearly seen with very little background. The curve is phase-space normalized to the total number of events.

decay, with the experimentally determined values of the density-matrix elements.

The same reaction has been studied¹³ at 2.24 GeV/c . The experimentally determined matrix elements were consistent both with the simple single-particle-exchange values given in Table I, and also with the absorption-model calculations with a modest form factor. Our results are consistent with small absorption corrections at 3.5 GeV/c also.

D. $K^-\bar{p} \rightarrow Y^*(1660)\pi^-$

Figure 7 shows the $\Sigma^-\pi^+\pi^+$ effective-mass distribution from the $\Sigma^-\pi^+\pi^+\pi^-$ final state. There is a sharp peak at about 1660 MeV which is largely retained on making a selection of events with momentum transfer to the π^- of less than 500 $(\text{MeV}/c)^2$. This peak is interpreted as peripheral production of the $Y^*(1660)$ resonance. An analysis of the decay Dalitz plot for this sample of $Y^*(1660)$ events, together with a similar number observed by the bubble-chamber groups at Saclay and École Polytechnique who studied the same reaction at 3.0 GeV/c , suggested a positive parity assignment¹⁴ for this resonance, and has been published previously.²

A search for the reaction $K^-\bar{p} \rightarrow Y^*(1660)\pi^-$ at a momentum transfer of less than 500 $(\text{MeV}/c)^2$ in various final states yielded the relative decay rates given in Table II. The inequalities there are quoted at the 90% confidence level. The $(\Sigma\pi/\Sigma\pi\pi)$ ratio is signifi-

TABLE I. Experimental values of the density-matrix elements, and values predicted from the Stodolsky-Sakurai model of $M_1 K^*$ exchange, for the decay of the $Y^*(1385)$ in the reaction $K^-\bar{p} \rightarrow Y^*(1385)\pi^-$.

	Experimental value	Predicted value
ρ_{33}	0.34 ± 0.06	0.375
$\text{Re}\rho_{31}$	0.00 ± 0.09	0.0
$\text{Re}\rho_{2-1}$	0.17 ± 0.09	0.217

¹³ G. W. London *et al.*, Phys. Rev. 143, 1034 (1966).

¹⁴ Our assignment agrees with that of Taher-Zadeh *et al.*, Phys. Rev. Letters 11, 470 (1963), but differs from that of D. Berley *et al.*, in *Proceedings of the Twelfth International Conference on High-Energy Physics, Dubna, 1964* (Atomizdat, Moscow, 1956), p. 565, and also from the results of London *et al.* (Ref. 13).

TABLE II. Branching ratios for the $Y_1^*(1660)$. The data are taken from the reaction $K^-\bar{p} \rightarrow Y_1^*(1660)\pi^-$ at a momentum transfer of less than 500 $(\text{MeV}/c)^2$. The total $(\Sigma\pi\pi)^+$ rate was obtained on the assumption that the decay is through $Y_0^*(1405)\pi^+$, so that the partial rates for decay to $(\Sigma^+\pi^+\pi^-)$, $(\Sigma^0\pi^0\pi^+)$, and $(\Sigma^-\pi^+\pi^+)$ are equal; the limit given for decay to $(\Sigma\pi)^+$ is obtained by using the $(\Sigma^+\pi^0)$ data only and multiplying by two. The limits correspond to 90% confidence levels.

Decay mode	Cross section (μb)	Relative rates		
		This expt.	Rosenfeld <i>et al.</i> ^a	London <i>et al.</i> ^b
$(\Sigma\pi\pi)^+$	32 ± 8	1	1	1
$(\Sigma\pi)^+$	< 14	< 0.4	~ 1	0.3 ± 0.15
$\Lambda\pi^+\pi^0$	11 ± 6	0.35 ± 0.2	~ 0.66	≤ 0.3
$\Delta\pi^+$	< 6	< 0.2	~ 0.16	< 0.3

^a Reference 15.

^b Reference 13.

cantly lower than that quoted by Rosenfeld *et al.*,¹⁵ but in agreement with the result obtained in an experiment at 2.24 GeV/c by London *et al.*¹³

E. $K^-\bar{p} \rightarrow Y^*\pi^0$

The $\Sigma^\mp\pi^\pm$ mass distributions in the $\Sigma^\mp\pi^\pm\pi^0$ final states (Fig. 8) show evidence for the production of three known isospin-zero hyperon resonances, $Y^*(1405)$, $Y^*(1520)$, and $Y^*(1815)$; there also appears to be an enhancement at 1645 MeV. The best fit to the distribution was obtained using a combination of Breit-Wigner curves and phase-space background with the results for the masses, widths, and partial rates as shown in Table III.

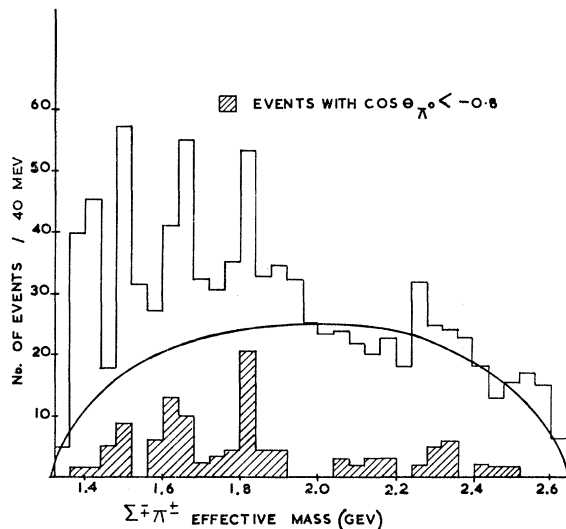


FIG. 8. The $\Sigma^\pm\pi^\mp$ effective-mass distribution for 613 events in the $\Sigma^\pm\pi^\mp\pi^0$ final states. The mean weighting factor is 1.49. The phase-space curve is normalized to the region above 2 GeV . The $Y^*(1405)$, $Y^*(1520)$, and $Y^*(1815)$ are evident. The interpretation of the enhancement in the 1660-MeV region is discussed in the text. The shaded events are those for which the cosine of the angle between the incident K^- and the outgoing π^0 is less than -0.8 (i.e., high-momentum transfer events).

¹⁵ A. H. Rosenfeld *et al.*, Rev. Mod. Phys. 37, 633 (1965).

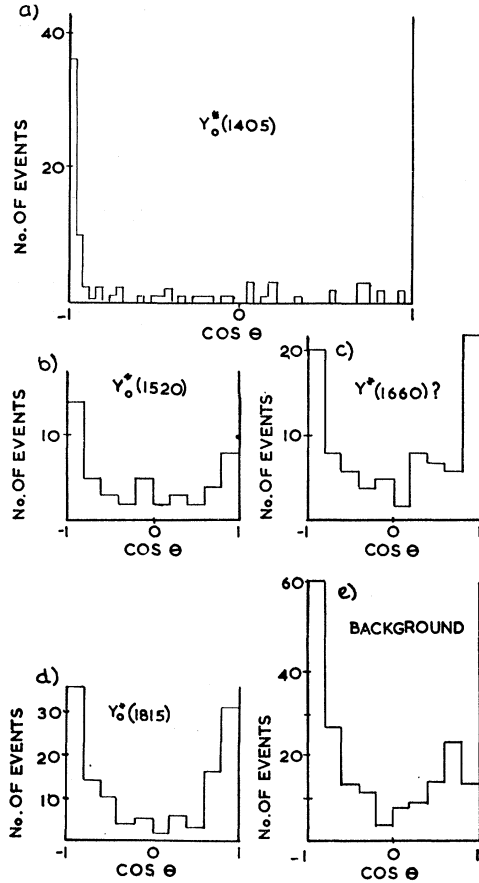


FIG. 9. Production angular distributions for various $\Sigma^\pm\pi^\mp$ combinations in the $\Sigma^\pm\pi^\mp\pi^0$ final states. (a) $\Sigma\pi$ mass in range (1.35 to 1.46) GeV. (b) $\Sigma\pi$ mass in range (1.49 to 1.53) GeV. (c) $\Sigma\pi$ mass in range (1.60 to 1.68) GeV. (d) $\Sigma\pi$ mass in range (1.75 to 1.89) GeV. (e) $\Sigma\pi$ mass below 2.01 GeV, and not included in (a) to (d). The region of the $Y^*(1405)$ is characterized by a sharp forward peak. The 1660- and 1815-MeV regions, on the other hand, appear to have significant backward peaks.

Center-of-mass production angular distributions for $(\Sigma\pi)^0$ combinations in the regions of the four peaks are shown in Fig. 9. Figure 9(e) includes all $\Sigma\pi$ combinations with mass below 2.01 GeV which are not plotted in Figs. 9(a) to (d). It is clear from this distribution [Fig. 9(e)] that backward peaking of the $(\Sigma\pi)^0$ combinations is a characteristic of the background. In contrast, Figs. 9(c) and 9(d), corresponding to the 1645-MeV enhancement

TABLE III. The masses, widths, and production rates of neutral Y^* 's as determined from maximum likelihood fits to the $\Sigma^\pm\pi^\pm + \pi^0$ final states.

Reaction	Mass (MeV)	Width (MeV)	Percentage of final states	Cross section (μb)
$Y^*(1405)\pi^0$	1400 ± 5	50 ± 10	11 ± 2	60 ± 10
$Y^*(1520)\pi^0$	1510 ± 2	16 ± 5	5 ± 1	30 ± 10
$Y^*(1660)\pi^0?$	1645 ± 6	40 ± 10	8 ± 2	40 ± 10
$Y^*(1815)\pi^0$	1810 ± 20	110 ± 50	8 ± 2	40 ± 10

TABLE IV. Cross sections (for decay by the modes specified in column 3) for the production of some of the more important of the two-body final states. In some of these cases a fit of the formula $d\sigma/d\Omega = Ke^{At}$ has been performed for momentum transfers less than $|t-t_0|_{\text{max}}$.

Channel	Cross section (μb)	Final state	A (GeV/c) $^{-2}$	$ t-t_0 _{\text{max}}$
$\Lambda\pi^0$	115 ± 40		3.3 ± 0.6	1.1
$\Sigma^+\pi^-$	140 ± 10		3.0 ± 0.5	1.0
$\Sigma^-\pi^+$	11 ± 3			
$Y^*(1385)\pi^-$	90 ± 15	$(\Lambda\pi^+)\pi^-$	2.4 ± 0.6	1.0
$Y^*(1405)\pi^0$	60 ± 10	$(\Sigma^\pm\pi^\mp)\pi^0$	12 ± 2	0.4
$Y^*(1520)\pi^0$	30 ± 10	$(\Sigma^\pm\pi^\mp)\pi^0$		
	9 ± 3	$(\Lambda\pi^+\pi^-)\pi^0$		
$Y^{*+}(1660)\pi^-$	21 ± 5	$(\Sigma^\pm\pi^\mp\pi^+)\pi^-$	3.7 ± 0.8	2.1
	11 ± 6	$(\Lambda\pi^+\pi^0)\pi^-$		
	< 7	$(\Lambda\pi^+)\pi^-$		
	< 14	$(\Sigma^+\pi^0\pi^+)\pi^-$		
$Y^*(1815)\pi^0$	40 ± 10	$(\Sigma^\pm\pi^\mp)\pi^0$		
$\Delta\eta$	5 ± 2	$\Lambda(\pi^+\pi^-\pi^0)$		
$\Delta\omega$	90 ± 10	$\Lambda(\pi^+\pi^-\pi^0)$	2.0 ± 0.4	2.4
$\Delta\Lambda^0$	20 ± 7	$\Lambda(\pi^+\pi^-\eta^0)$		
$\Delta\phi$	40 ± 15	$\Lambda(K\bar{K})$	1.9 ± 0.3	1.7
$\Sigma^+\rho^-$	150 ± 20	$\Sigma^+(\pi^-\pi^0)$	3.3 ± 0.6	1.0
$\Sigma^+A_2^-$	20 ± 5	$\Sigma^+(\rho^0\pi^-)$		
Ξ^-K^+	16 ± 5			
Ξ^-K^*	16 ± 4	$\Xi^-(K^+\pi^0\pi^+)$		

and $Y^*(1815)$ regions, respectively, show a marked forward peaking, absent in Fig. 9(e), and which may be the result of a baryon-exchange contribution to the production of these $(\Sigma\pi)^0$ states. The shaded histogram in Fig. 8 shows those events with high momentum transfers to the $\Sigma^\mp\pi^\pm$ combination, corresponding to backward production angles ($\cos\theta_{\pi^*} < -0.8$) for the π^0 . The peak to background ratio is seen to be enhanced both in the 1645-MeV region and even more strikingly in the $Y^*(1815)$ region. In contrast to this, the $Y^*(1405)$ shows a backward peaking typical of one-meson-exchange production processes. In fact, the forward meson peak for the reaction $K^-p \rightarrow Y^*(1405)\pi^0$ is sharper than that for any other reaction in this experiment (see Table IV).

The level of background under the $Y_0^*(1405)$ peak is low (Fig. 10), but the folded Treiman-Yang distribution for events in the $Y_0^*(1405)$ region contains a large concentration of events in the region of $\phi=0$. The asymmetry about 90° indicates the presence of interference

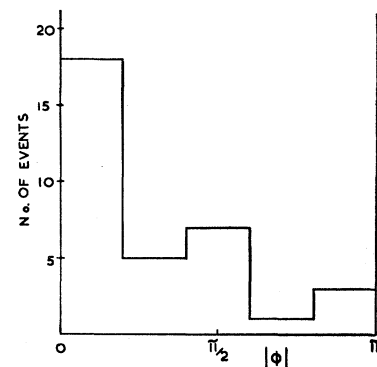


FIG. 10. The folded Treiman-Yang distribution for events in the $Y^*(1405)$ from the final state $Y^*\pi^0$. The lack of symmetry about $\frac{1}{2}\pi$ indicates the presence of interference effects.

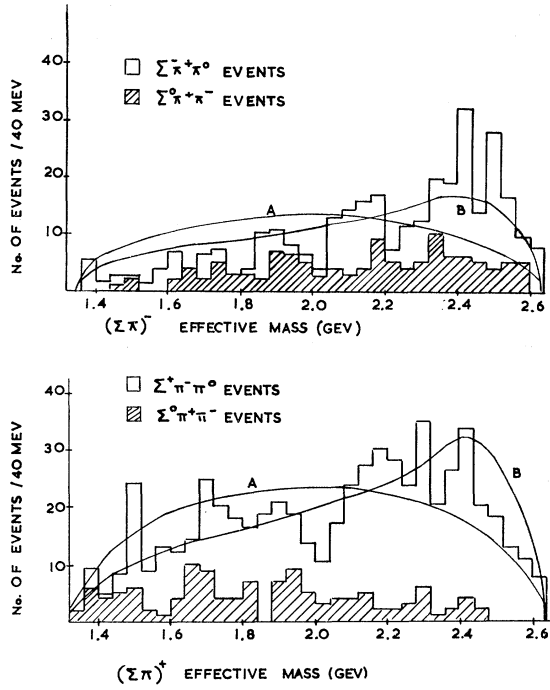


FIG. 11. The $(\Sigma\pi)^-$ and $(\Sigma\pi)^+$ effective-mass distributions in the $\Sigma^- \pi^0 \pi^0$, $\Sigma^- \pi^+ \pi^-$, $\Sigma^+ \pi^0 \pi^0$, $\Sigma^+ \pi^+ \pi^-$ final states. There are 124 events in the $\Sigma^0 \pi^+ \pi^-$ final state (unweighted), 247 events in the $\Sigma^- \pi^+ \pi^0$ final state (mean weighting factor = 1.29), and 366 events in the $\Sigma^+ \pi^- \pi^0$ final state (mean weighting factor = 1.63). The curves A are phase-space-normalized to the total number of events in the distributions, while the curves B include the reflections of the three neutral Y^* resonances and the 1645-MeV enhancement.

effects which prevent us from attempting to confirm the indirect spin-parity assignment¹⁶ of $\frac{1}{2}^-$ for the $Y^*(1405)$.

The $Y^*(1520)$ is also seen in the $\Lambda\pi^+\pi^-$ decay mode in the $\Lambda\pi^+\pi^-\pi^0$ final state. The branching ratio is found to be

$$\frac{Y^*(1520) \rightarrow \Lambda\pi^+\pi^-}{Y^*(1520) \rightarrow \Sigma^\pm\pi^\mp} = 0.3 \pm 0.1,$$

in agreement with the value given in Ref. 15. The level of background under the $Y_0^*(1520)$ peak is large and no attempt has been made to examine its decay distributions.

F. The 1645-MeV Enhancement

The curve drawn in Fig. 8 is phase-space-normalized in the region of $\Sigma\pi$ mass above 2.0 GeV, and is seen to give an adequate fit in this region. Apart from the $Y^*\pi^0$ channels, the only strong resonant channel in the $\Sigma^\pm\pi^\mp\pi^0$ final states is $\Sigma^+\rho^-$, and it is found to produce no appreciable distortions of the background in the $\Sigma^\pm\pi^\mp$ mass distribution.¹⁷ Therefore, in the following discussion we use the phase-space curve normalized in the

¹⁶ J. Kim, Phys. Rev. Letters 14, 29 (1965).

¹⁷ In fact if the ρ^- events are removed and the phase space curve is renormalized, the statistical significance of the 1645-MeV enhancement is, if anything, increased.

region above 2.0 GeV to give an estimate of the background in the region below 2.0 GeV, where all the resonant effects occur.

Figure 11 shows the $\Sigma^- \pi^0 \pi^0$ and $\Sigma^+ \pi^0 \pi^0$ distributions from the $\Sigma^- \pi^0 \pi^0$ and $\Sigma^+ \pi^0 \pi^0$ final states, while in Fig. 12 are the corresponding Dalitz plots. The curves A in Fig. 11 are phase-space curves normalized to the total number of events in the distributions, while the curves B include the reflections of the three neutral Y^* resonances and the 1645 enhancement. A further peaking is expected at high mass values due to the contamination ($\sim 13\%$) of $\Sigma^\pm\pi^\pm\pi^0\pi^0$ events in the sample (see Appendix A.2).

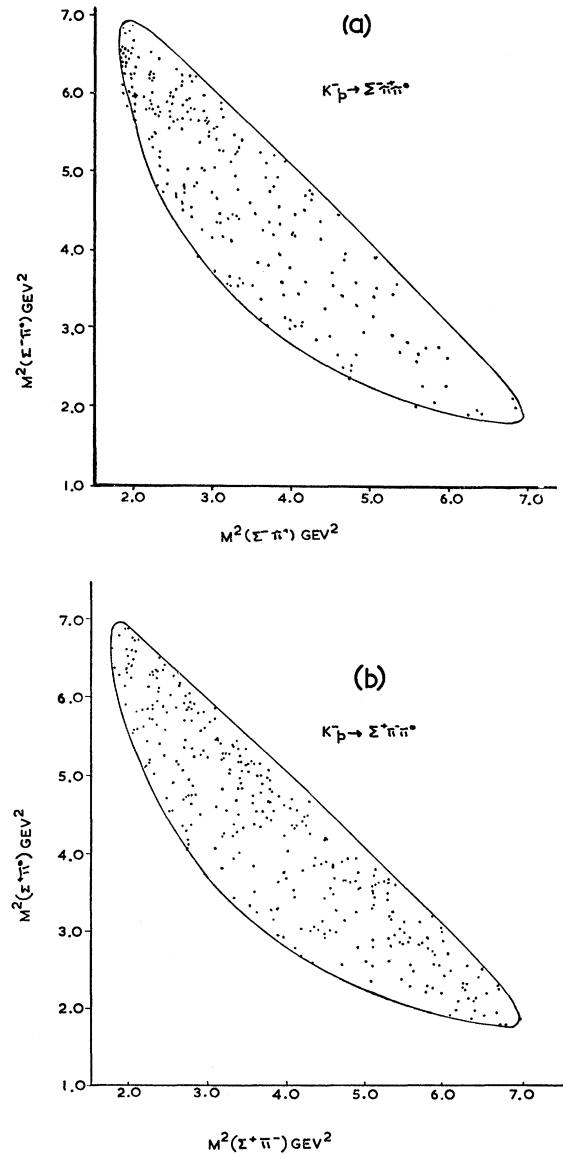


FIG. 12. Dalitz plots (a) for the $\Sigma^- \pi^+ \pi^0$ final state, and (b) for the $\Sigma^+ \pi^- \pi^0$ final state.

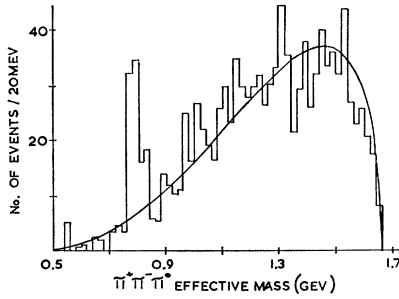


FIG. 13. The effective-mass distribution of $\pi^+\pi^-\pi^0$ from 1013 $\Lambda\pi^+\pi^-\pi^0$ events, whose mean weighting factor is 1.15. The curve shown is phase-space normalized to the region outside the ω peak. The final state $\Delta\eta$ is only weakly produced.

We now discuss the significance of the enhancement at 1645 MeV and its possible relationship to the $Y_1^*(1660)$.

(i). There are 96 events in the 1600–1680-MeV mass region, compared with a background expectation, estimated as described above, of 43 events; the excess corresponds to an eight-standard-deviation effect.

(ii). The $Y_1^*(1660)$ has been observed in this experiment by its $\Sigma\pi\pi$ decay mode, and thus we expect to obtain some $Y_1^{*0}(1660)$, which could decay into $\Sigma^\pm\pi^\mp$. We can estimate the expected number of such events from the observed number of $\Sigma^-\pi^+\pi^+$ decays if we assume: (a). The ratio of Y^{*+} to Y^{*0} is 4, as expected from the exchange of an isospin- $\frac{1}{2}$ strange boson.¹⁸ (b). The $\Sigma\pi\pi$ decays of the $Y^*(1660)$ are dominated by the $Y^*(1405)\pi$ channel.¹⁹ (c). The ratio of $(Y^*(1660) \rightarrow \Sigma\pi\pi)/(Y^*(1660) \rightarrow \Sigma\pi)$ is about unity.¹⁵ Then the contribution made by the decay of the $Y^{*0}(1660)$ to $\Sigma^\pm\pi^\mp$ is estimated as 14 events. This is insufficient to account for our enhancement; an excess of ~ 5 standard deviations remains.

(iii). Alternatively, we can use assumption (a) above to make a direct comparison of the $(\Sigma\pi)^+$ and $(\Sigma\pi)^0$ rates in the 1660-MeV region. As can be seen from Fig. 11, we have little evidence for an enhancement in the $(\Sigma\pi)^+$ effective mass at 1660 MeV, and the upper limit that we can put on the expected $(\Sigma\pi)^0$ contribution from the decay of the $Y_1^*(1660)$ is lower than the estimate given in (ii).

(iv). Another contrasting feature is the production angular distribution: Whereas the $Y^{*+}(1660)$ seen in the $\Sigma\pi\pi$ mode is produced peripherally [almost all events having a momentum transfer of less than 0.5 $(\text{GeV}/c)^2$], the enhancement at 1645 MeV is associated with forward production of $(\Sigma\pi)^0$ states. [See Figs. 7 and 9(c).]

¹⁸ If we do not assume a single-particle exchange model, this condition can be replaced by a triangular inequality

$$(\sigma(Y^{*+}\pi^-))^{1/2} + (\sigma(Y^{*0}\pi^+))^{1/2} \geq 2(\sigma(Y^{*0}\pi^0))^{1/2}.$$

This slightly weakens the argument that the observed excess of events in the 1645-MeV region is incompatible with that expected from the two-body decay of the $Y^*(1660)$.

¹⁹ P. Eberhard *et al.*, Phys. Rev. Letters **14**, 466 (1965).

Thus, there are difficulties in attempting to account for the enhancement in terms of the $Y^*(1660)$ of isospin one. If we were to interpret this enhancement in terms of a hyperon resonant state, its isospin would presumably be zero, since it is observed only in the neutral state. Its mass and width are given in Table II. This mass is lower than the value of 1670 MeV given by Berley²⁰ for the isospin-zero resonant state through which the reaction $K^-p \rightarrow \Lambda\eta$ proceeds near threshold.

G. $K^-p \rightarrow \Lambda\omega, \Lambda\eta, \Lambda X^0$

Figure 13 shows the $\pi^+\pi^-\pi^0$ effective-mass distribution in the $\Lambda\pi^+\pi^-\pi^0$ final state. The ω is produced with quite low background and with a cross section of $90 \pm 10 \mu\text{b}$. Figure 14 shows the production angular distribution for events in the ω region [$0.76 \text{ GeV} < M(\pi^+\pi^-\pi^0) < 0.8 \text{ GeV}$]. In addition to the pronounced forward peaking expected on a peripheral-production model, there is a definite backward peak which is possibly associated with a baryon-exchange mechanism. A similar backward peaking has been observed in the same channel at 2.7, 3.0, and 6 GeV/c.^{21,27}

Choosing events in which the ω is produced in the forward direction [$\Delta^2 < 700 (\text{MeV}/c)^2$], the following values are obtained for the decay density matrix elements:

$$\rho_{00} = 0.28 \pm 0.15; \quad \rho_{1-1} = 0.15 \pm 0.1; \\ \text{Re}\rho_{10} = 0.08 \pm 0.08.$$

On the simple single-particle-exchange model, the value of ρ_{00} would imply that vector exchange is more important than pseudoscalar exchange for this reaction. An absorption-model calculation for pure K exchange,

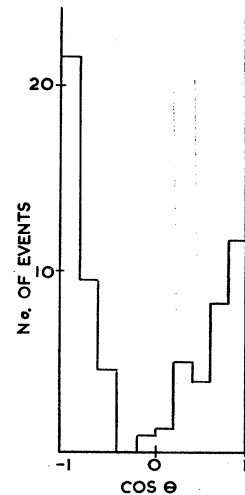


FIG. 14. The center-of-mass production angular distribution for 55 $\Lambda\omega$ events (defined by the $\pi^+\pi^-\pi^0$ effective mass being between 760 and 800 MeV). As well as the usual forward meson peak, there is also a significant backward one which is absent from the corresponding plot for the $\Delta\phi$ final state (see Fig. 16).

²⁰ D. Berley *et al.*, Phys. Rev. Letters **14**, 641 (1965), who state that they have no evidence for any $\Sigma\pi$ decay modes of this resonance.

²¹ R. Ross, in *Proceedings of the Twelfth International Conference on High-Energy Physics, Dubna, 1964* (Atomizdat, Moscow, 1965), p. 642; R. Sekulin (private communication).

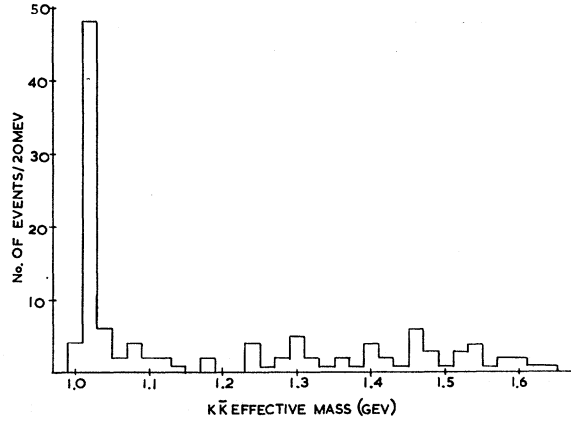
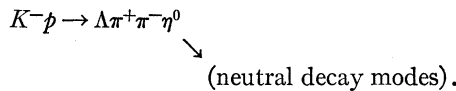


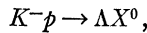
FIG. 15. The $K\bar{K}$ effective-mass distribution for 120 events identified as ΔK^+K^- or $\Delta K_1^0K_2^0$.

however, gives a value of ρ_{00} of 0.28, and hence it is not possible to make any firm statement about the nature of the exchanged particle.

It may also be seen from Fig. 13 that the η is produced, but with the small cross section of $\sim 5 \mu\text{b}$ for decay into the $\pi^+\pi^-\pi^0$ mode. Events of the topology $\Lambda+2$ prongs were examined for evidence of missing η^0 ; that is, for the reaction,



The $\eta\pi^+\pi^-$ spectrum then showed evidence of X^0 production, 18 events being seen above a phase-space prediction of 3 events. This corresponds to a cross section of $20 \pm 7 \mu\text{b}$ for the reaction



followed by the $\eta\pi^+\pi^-$ decay mode of the X^0 .

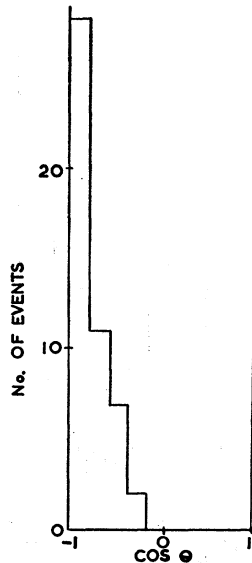


FIG. 16. The center-of-mass production angular distribution for 48 $\Lambda\phi$ events, defined by the $K\bar{K}$ mass being between 1.01 and 1.03 GeV. The distribution contains 23 K^+K^- and 25 $K_1^0K_2^0$ combinations.

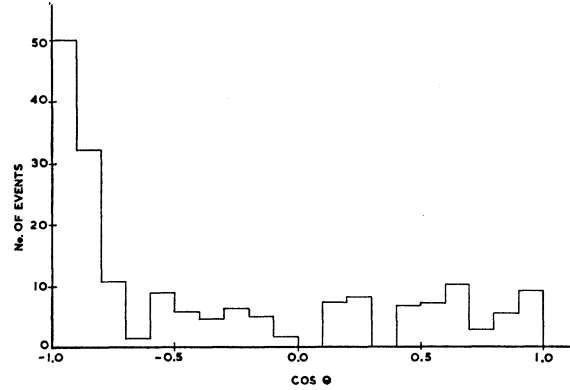


FIG. 17. The production angular distribution for $\Sigma^+\rho^-$ events. Events with $\pi^-\pi^0$ mass in the range 670–870 MeV have been included in the histogram.

H. $K^-p \rightarrow \Lambda\phi$

The $K\bar{K}$ effective mass distribution from the final states ΔK^+K^- and $\Delta K_1^0K_2^0$ is shown in Fig. 15. The ϕ is strongly produced with very low background, and a width comparable to the experimental resolution. The cross section for the $\Lambda\phi$ channel is $40 \pm 15 \mu\text{b}$. The production angular distribution for events (Fig. 16) in the ϕ peak shows the marked forward peaking also seen in ω production, but the backward peak present in ω production is entirely absent for the ϕ ; indeed, there are no events in the backward hemisphere. In terms of a baryon-exchange model, this implies that $g_{pp\omega}$ is much larger than $g_{pp\phi}$, as expected if the ω is identified with the particle that contributes most strongly to the isoscalar-nucleon form factor.

The density-matrix elements for the decay of the ϕ are:

$$\rho_{00} = 0.37 \pm 0.16; \quad \rho_{1-1} = 0.0 \pm 0.1; \\ \text{Re}\rho_{10} = 0.06 \pm 0.06.$$

The value of ρ_{00} predicted by the absorption model for pure K exchange is 0.4, and hence, as in the $\Lambda\omega$ reaction, it is not possible to draw any conclusion concerning the spin of the exchanged particle.

I. $K^-p \rightarrow \Sigma^+\rho^-$

As may be seen from the Dalitz plots of the $\Sigma^\pm\pi^\mp\pi^0$ final states, the production of $\Sigma^+\rho^-$ is very much stronger than that of $\Sigma^-\rho^+$; the cross section for the former is found to be $150 \pm 20 \mu\text{b}$. Furthermore, the production angular distribution (Fig. 17) of $\Sigma^+\rho^-$ is sharply peaked, which is not the case for $\Sigma^-\rho^+$. This is, of course, not surprising if the reaction is dominated by K and/or K^* exchange.

On selecting events with the mass of the $\pi^-\pi^0$ combination between 670 and 870 MeV, and having momentum transfer to the Σ^+ below 600 $(\text{MeV}/c)^2$, the values determined for the elements of the density matrix

describing the ρ^- decay were²²:

$$\rho_{00} = 0.17 \pm 0.08; \quad \rho_{1-1} = 0.17 \pm 0.08;$$

$$\text{Re}\rho_{10} = 0.01 \pm 0.04.$$

Without absorption effects a value of zero for ρ_{00} would correspond to K^* exchange but again the data could be consistent with a large proportion of K exchange. The prediction of A -parity²³ is that K exchange should be more important than K^* exchange.

J. $K^-p \rightarrow \Sigma^+ A_2^-$

The final states $\Sigma^\pm \pi^\mp \pi^+ \pi^-$ show strong evidence for ρ^0 production. Dalitz plots of the $\Sigma^\pm \pi^\mp \rho^0$ events (defined as having a $\pi^+ \pi^-$ mass between 675 and 825 MeV) are shown in Fig. 18. The $Y^*(1520)$ is clearly seen in both the Dalitz plots. In Fig. 18(a), a band corresponding to the production of A_2^- is evident, but the A_2^+ band in Fig. 18(b) shows an increased density only in the region where the $Y^*(1520)$ band crosses it. The production of $\Sigma^+ A_2^-$, but not of $\Sigma^- A_2^+$, is again consistent with a meson-exchange process.

If the A_1 is produced, it is certainly much weaker than the A_2^- (Fig. 19). This would not be surprising if the A_1 were a kinematic enhancement associated with the Deck process.²⁴

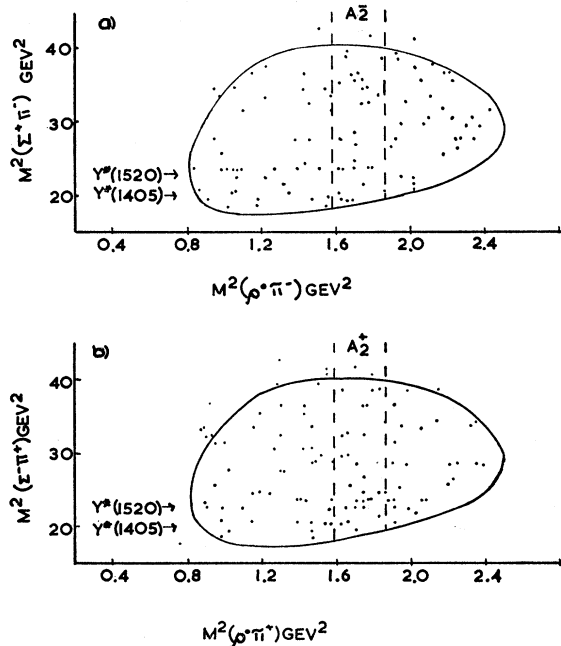


FIG. 18. Dalitz plots for the final states (a) $\Sigma^+ \rho^0 \pi^-$ and (b) $\Sigma^- \rho^0 \pi^+$. The A_2^- shows up as a band in (a), but the A_2^+ appears in (b) only in the cross-over region with the $Y^*(1520)$.

²² Similar values for the density matrix elements of the decay of the ρ^0 have been observed by E. D. Aleya, Jr., *et al.*, Phys. Letters 15, 82 (1965), who studied the reaction $K^-n \rightarrow \Sigma^- \rho^0$ at 2.24 GeV/c.

²³ J. B. Bronzan and F. E. Low, Phys. Rev. Letters 12, 522 (1964).

²⁴ R. T. Deck, Phys. Rev. Letters 13, 169 (1964).

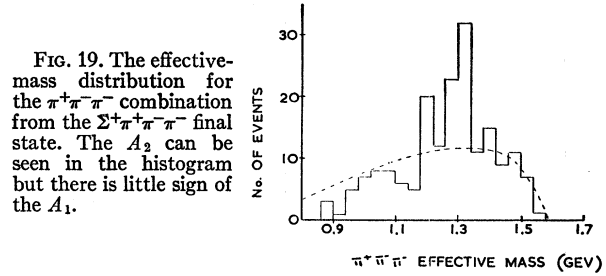


FIG. 19. The effective-mass distribution for the $\pi^+ \pi^- \pi^-$ combination from the $\Sigma^+ \pi^+ \pi^- \pi^-$ final state. The A_2 can be seen in the histogram but there is little sign of the A_1 .

K. $K^-p \rightarrow \Xi^- K^+$ and $\Xi^- K^*$

The cross sections for the channels $\Xi^- K^+$ and $\Xi^- K^{*+}$ are $16 \pm 5 \mu\text{b}$ and $16.5 \pm 4 \mu\text{b}$, respectively. The production angular distributions for the Ξ^- in these final states are shown in Figs. 20 and 21. As observed at lower beam momenta,^{13,25-27} the Ξ^- is produced preferentially at high-momentum transfers, as expected if baryon exchange contributes to the production. The background under the K^{*+} peak is considerable, and so no decay-correlation analysis has been performed.

There is only weak evidence for the production of the final states $\Xi^* K$. The upper limit we can set on the cross section for $\Xi^{*0} K^0$ is $10 \mu\text{b}$.

4. CONCLUSIONS

The most striking feature of the data is that the two-body final states very often show a high degree of peripheralism. With a few exceptions, those reactions for which meson exchange is allowed are characterized by a sharp forward peak of the outgoing meson. The present level of statistical accuracy prevents our making any detailed comments on the differences in the shapes of these peaks for the various final states (see Table IV). They do, however, appear to be somewhat more shallow than either the K^-p elastic scattering cross section or

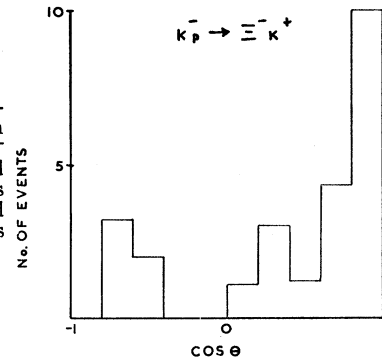


FIG. 20. The production angular distribution of 17 events of the $\Xi^- K^+$ final state. The forward peaking of the cascade is similar to that observed at other momenta in this reaction.

²⁵ L. W. Alvarez, in *Proceedings of the 1962 Annual International Conference on High-Energy Nuclear Physics at CERN*, edited by J. Prentki (CERN, Geneva, 1962), p. 433.

²⁶ H. Ticho, in *Proceedings of the 1962 Annual International Conference on High-Energy Nuclear Physics at CERN*, edited by J. Prentki (CERN, Geneva, 1962), p. 436.

²⁷ J. Badier *et al.*, in *Proceedings of the Oxford International Conference on Elementary Particles, 1965* (Rutherford High Energy Laboratory, Harwell, England, 1966), supplement, p. 70.

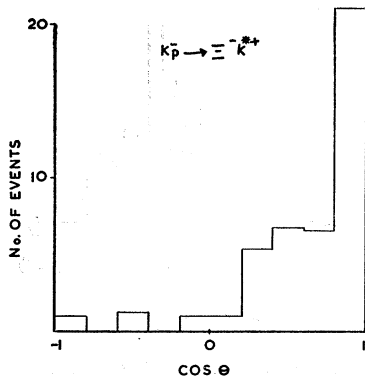


FIG. 21. The production angular distribution of 33 events of the $\Xi^- K^*$ final state, the K^* being defined by the mass range 840–950 MeV. As in the $\Sigma^- \pi^+$ and $\Xi^- K^+$ final states which are also forbidden for meson exchange, a forward peaking of the final state baryon is evident.

the majority of the angular distributions in $\pi^\pm p$ final states.

On the other hand, in those reactions for which there exists no suitable meson to be exchanged, the cross sections are much smaller, and the production is characterized by a backward peak in the outgoing meson's production angular distribution; the final states $\Xi^- K^+$, $\Xi^- K^*$, and $\Sigma^- \pi^+$ are examples of this effect. Similar backward meson peaks are evident in some reactions for which there is also a forward meson peak; the $\Lambda\omega$ and $Y^*(1815)\pi^0$ final states provide examples of this. This effect may possibly be interpreted in terms of a baryon-transfer process.

The decay distribution of $Y^*(1385)$ in the $Y^*\pi^-$ final state was seen to be in good agreement with the predictions of the Stodolsky-Sakurai model for $M1 K^*$ exchange. Those reactions ($\Sigma^+\rho^-$, $\Lambda\omega$, and $\Lambda\phi$) for which a mixture of K and K^* exchange is allowed are characterized by fairly small values of ρ_{00} for the vector-meson decay. It is difficult, however, to regard this as strong evidence for the dominance of vector exchange, since the situation is complicated by the fact that the absorption model applied to the case of pure K exchange also predicts small values of ρ_{00} .

Although it appeared from the $\Sigma^\pm\pi^\mp$ mass distribution that our sample of $Y^*(1405)$ did not suffer from a large background of nonresonant events, the decay distribution indicated that the background was important, and precluded any attempt at a direct spin-parity determination.

Finally, an enhancement was observed at 1645 MeV in the $\Sigma^\pm\pi^\mp$ systems, which was difficult to explain in terms of the decay of the neutral $Y^*(1660)$.

A summary of the cross sections, decay modes, and production angular distributions of some of the two-body reactions observed in this experiment is provided in Table IV. Our data and that of Ref. 3 show the usual decrease in cross section for producing baryons of decreasing strangeness in two-body reactions. The cross sections in the more favorable cases are about 500, 100, and $10 \mu\text{b}$ for baryons of strangeness 0, -1 , and -2 , respectively.

ACKNOWLEDGMENTS

We wish to thank all who helped in obtaining data for this experiment, in particular the Deutsches Rechenzentrum, Darmstadt, the Imperial College computing laboratory, the Atlas laboratory, the staffs of the CERN proton synchrotron and of the Saclay 81-cm bubble chamber, and finally the scanning and measuring staff of the various laboratories. We are also indebted to R. Keyser for advice and help with the absorption-model calculations.

APPENDIX A: WEIGHTING FACTORS

Events containing Λ 's or Σ 's were weighted to allow for the fact that some of the hyperons would be lost because they decayed too near to the production vertex to be clearly identified, or because they decayed outside the visible volume of the bubble chamber, or, in the case of Σ 's, because the decay angle was too small. The corrections for Λ 's and for Σ 's were made by slightly different methods, and are considered separately below.

1. Events Containing Λ 's

For each event involving a Λ , the potential path L available within the scanning region for a Λ of the observed direction and coming from the observed production vertex was calculated. A correction was then applied to allow for the fact that Λ 's could decay after distance L , and hence be lost or rejected. Furthermore, events with a Λ path length δ less than 0.5 cm were rejected; this effect was more important for slow Λ 's.

To compensate for these missing Λ 's, each observed event was weighted by a factor W , where

$$1/W = e^{-\delta/\lambda} - e^{-L/\lambda},$$

where λ is the mean-decay length. The average values of this weighting factor for all Λ 's was 1.16.

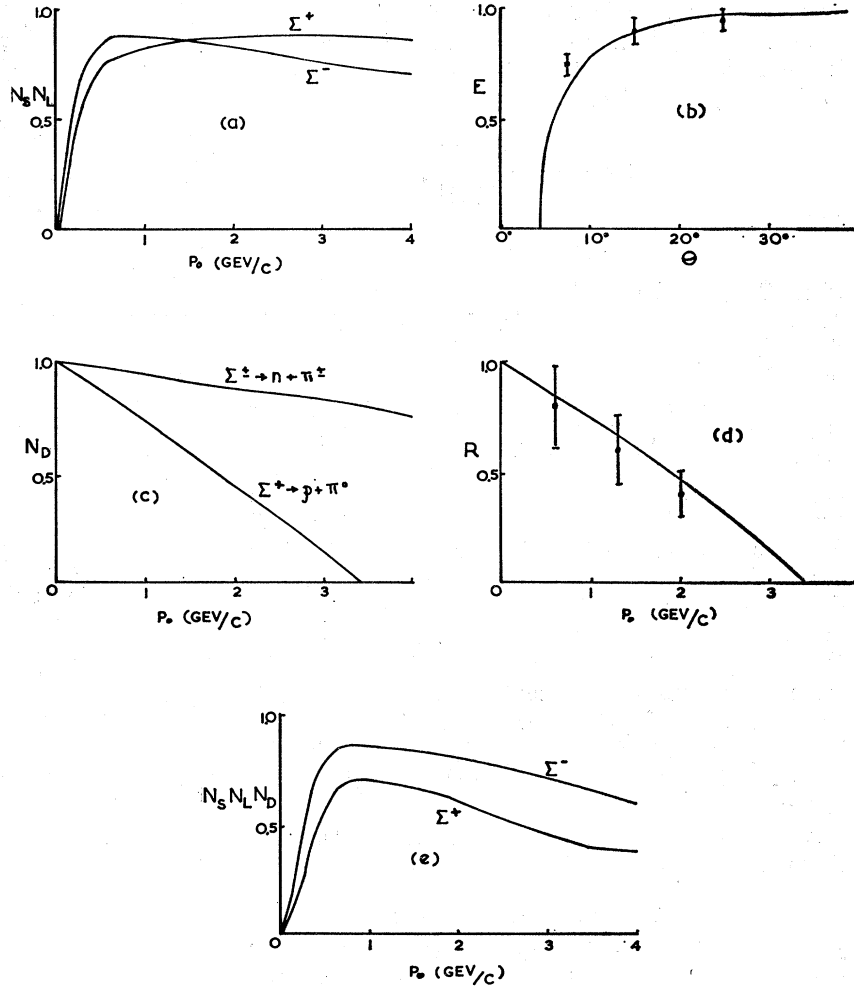
2. Events Containing Σ^\pm

A slightly different approach was used for Σ 's. The weighting factor for each event was calculated only as a function of the momentum of the Σ , being already averaged over all the other relevant variables. This method was used in this case to avoid the danger of the weighting factors for particular events becoming excessively large. (The average correction to be applied to Σ events was considerably larger than that for events with Λ 's; see below.) The weighting factor was corrected for three different sources of loss.

i. Short Decays

A plot of the number of Σ 's observed as a function of decay distance x , weighted by the usual factor $\exp(x/\lambda(p))$, was consistent with all events with x greater than 0.4 cm being seen, while essentially no events had x smaller than 0.2 cm. It was thus assumed

FIG. 22. (a) The efficiency $N_s N_L$ for detecting Σ^+ and Σ^- decays as a function of momentum, the losses being due to decay outside the chamber and within 0.5 cm of the production vertex. (b) The efficiency E for observing decays in the unfavorable azimuthal region as a function of decay angle. The curve is calculated on the assumption that decays will be observed if the angle as seen by at least one of the cameras is greater than 4° . (c) The efficiency N_D for detecting $\Sigma^+ \rightarrow p\pi^0$ or $\Sigma^\pm \rightarrow n\pi^\pm$ decays as a function of momentum, loss being due to small angle decays. For $\Sigma^+ \rightarrow p\pi^0$ above 3.4 GeV/c, all decays are less than 4° . (d) The ratio R of $(\Sigma^+ \rightarrow p\pi^0)/(\Sigma^+ \rightarrow n\pi^+)$ as observed as a function of momentum. The curve is the calculated ratio of the detection efficiencies of the two modes as obtained from (c). (e) The product of the efficiencies in (a) and (c), the reciprocals of which give the weighting factors. The discontinuity in the Σ^+ curve at 3.4 GeV/c arises from the fact that the $\Sigma^+ \rightarrow p\pi^0$ decay mode cannot be observed above this momentum.



that the efficiency for observing short decays was

$$E_s = \begin{cases} 0, & \text{for } x < l_0 = 0.2 \text{ cm} \\ = (x - l_0)/(l_1 - l_0), & \text{for } l_0 \leq x \leq l_1 \text{ cm} \\ = 1, & \text{for } x > l_1 = 0.4 \text{ cm}. \end{cases}$$

Then for a given momentum p , the efficiency averaged over all possible values of x will be

$$N_s(p) = \frac{1}{N_2} \int_0^\infty E_s \frac{dN}{dx} dx \\ = \frac{\lambda}{l_1 - l_0} e^{-(l_0/\lambda)} [1 - e^{-(l_1 - l_0)/\lambda}],$$

where

$$dN/dx = (N_0/\lambda) e^{-x/\lambda}.$$

ii. Long Decays

Decays were accepted if they occurred either within the accepted fiducial region of length $L = 40$ cm, or within a distance ΔL of 7 cm beyond it. The efficiency

for observing decays is then²⁸

$$E_L = 1 - e^{-(L + \Delta L - x)/\lambda},$$

where x is the position of the production vertex of the event as measured from the beam end of the fiducial region. Then, on averaging over x , we obtain

$$N_L(p) = 1 - (\lambda/L) [e^{-\Delta L/\lambda} - e^{-(L + \Delta L)/\lambda}].$$

Figure 22(a) shows the efficiency as a function of momentum for detecting Σ^+ and Σ^- decays after allowing for effects *i* and *ii*. The difference between the two charged states arises because the Σ^- has a longer lifetime.

iii. Small-Angle Decays

Sigmas decaying through a small angle may easily be missed on the scanning table. The importance of this effect was estimated by calculating for each observed

²⁸ The implicit approximation that the Σ 's are traveling along a direction perpendicular to the ends of the scanning box (i.e., parallel to the beam direction) is not seriously in error, especially as the correction for the loss of fast Σ 's is small.

event the decay angle θ and the azimuthal angle ϕ , defined as being the angle between the horizontal which is perpendicular to the sigma direction and the normal to the decay plane, i.e.,

$$\cos\phi = \frac{(\hat{\Sigma} \times \hat{\pi}) \cdot (\hat{\Sigma} \times \hat{z})}{|\hat{\Sigma} \times \hat{\pi}| |\hat{\Sigma} \times \hat{z}|},$$

and

$$\cos\theta = \hat{\Sigma} \cdot \hat{\pi},$$

where $\hat{\Sigma}$, $\hat{\pi}$, and \hat{z} are unit vectors along the Σ , charged decay particle, and vertical directions, respectively, in the laboratory. Then the distribution in ϕ should be isotropic.

A plot of the number of events as a function of ϕ for given intervals of θ indicated that events with small values of θ were being lost in the unfavorable (small) ϕ region, whereas for θ greater than 30° , the loss was negligible. In this way an efficiency for observing small ϕ events was estimated empirically for several values of θ , and was found to be consistent with the assumptions that events were observed only if the decay angle as seen by at least one of the cameras was greater than 4° [see Fig. 22(b)]. The efficiency of detecting small-angle decays was then calculated as a function of Σ momentum assuming that 4° was the minimum observable decay angle. This efficiency N_D is plotted in Fig. 22(c) for the proton and for the charged pion-decay modes.

A check on this calculation was obtained by observing that the experimental ratio

$$R = [\Sigma^+ \rightarrow p\pi^0] / [\Sigma^+ \rightarrow n\pi^+]$$

agreed well with the ratio of the detection efficiencies of the proton and charged pion-decay modes [Fig. 22(d)]. The over-all efficiency for detecting the decay of charged Σ 's is then simply the product $N_s N_L N_D$, and is shown in Fig. 22(e). Each event was then weighted by the relevant weighting factor $W(p)$, where

$$1/W = N_s N_L N_D.$$

APPENDIX B: PURITY OF SAMPLES

1. Events Involving Σ^\pm

On the subsample of film, a careful investigation was made of the various sources of contamination in the events $K^-p \rightarrow \Sigma^\pm + \text{pion}(s)$. There are three main types of contamination.

(i). Kinematic ambiguities between reactions of the type $K^-p \rightarrow \text{one strange particle} + \text{nonstrange particle}(s)$. The following hypotheses were used for 2-prong Σ events.

$$\begin{aligned} K^-p &\rightarrow \Sigma^\pm \pi^\mp, \\ &\Sigma^\pm \pi^\mp \pi^0, \\ &K^-p, \\ &K^-p\pi^0, \\ &K^-n\pi^+. \end{aligned}$$

TABLE V. Ambiguities for Σ final states. The second column refers to events which were consistent kinematically and from the point of view of ionization with only one of the 7 hypotheses listed in (i) of Appendix A.2. Events which also gave a fit to $K^-n\pi^+$ or to $K^-n\pi^+\pi^-\pi^+$ are listed in column 4; almost all of these are Σ^- events, and so should be added to the number listed in column 2. Other ambiguities are listed in column 3. The estimated contamination from events with more than one missing neutral, appears under column 5, while the total number of events with two or more strange particles which could fit the different hypotheses is given in the last column.

Final state	Unique	Amb 1	Amb 2	$2\pi^0$	≥ 2 st. parts
$\Sigma^+\pi^-$	55	0	0		
$\Sigma^-\pi^+$	4	1	1		
$\Sigma^+\pi^-\pi^0$	134	0	0	15%	$\lesssim 8$
$\Sigma^-\pi^+\pi^0$	90	3	19	11%	$\lesssim 24$
$\Sigma^+\pi^+\pi^-\pi^-$	74	1	0	$< 3\%$	~ 0
$\Sigma^-\pi^-\pi^+\pi^+$	69	0	0	$< 3\%$	$\lesssim 10$

For 4-prong Σ 's, the list was as above, but with a $\pi^+\pi^-$ pair added to each final state.

After the ionization of the tracks had been examined for consistency with the fitted hypotheses, 87% of the events gave a unique fit, the main ambiguity remaining being between the final states $K^-n\pi^+$ and $\Sigma^-\pi^+\pi^0$; the number of these events is listed in Table V in the column "Amb 2." An examination of the lifetime distribution of the negative decaying tracks showed that at most 3 or 4 of these 20 events could be kaons, and they were consistent with being all Σ^- , so the number of unambiguous fits should be increased accordingly. The remaining ambiguities are included in the column "Amb 1."

(ii). Events with two missing π^0 's can sometimes fit the corresponding hypotheses with one missing π^0 . The importance of this effect was estimated by using events from the final states $\Sigma^\pm \pi^\mp \pi^+\pi^-$ as fake $\Sigma^\pm \pi^\mp \pi^0\pi^0$ events.²⁹ These were then fitted in the same way as the 2-prong Σ events. Then if we assume that the cross sections

$$\sigma(\Sigma^+\pi^-\pi^0\pi^0) \approx \sigma(\Sigma^+\pi^-\pi^+\pi^-),$$

and

$$\sigma(\Sigma^-\pi^+\pi^0\pi^0) \approx \sigma(\Sigma^-\pi^+\pi^+\pi^-),$$

the estimated contamination of the $\Sigma^\pm \pi^\mp \pi^0$ final states³⁰ are as shown in the " $2\pi^0$ " column of Table V.

(iii). Finally, there is the contamination arising from the final states containing two or more strange par-

²⁹ For 4-prong Σ events the contamination from two missing π^0 's is not important, since the ratio of 6-prong to 4-prong Σ 's found in this experiment is small ($\sim 3\%$).

³⁰ The most serious bias that can be introduced by $\Sigma^\pm \pi^\mp \pi^0\pi^0$ events fitting the hypothesis $\Sigma^\pm \pi^\mp \pi^0$ is that the (incorrect) fitted $\Sigma^\pm \pi^0$ mass may not be very different from the true $\Sigma^\pm \pi^0\pi^0$ mass. Thus a three-body decay mode of the $Y^*(1660)$ could cause a spurious peak in the $\Sigma^\pm \pi^0$ mass spectrum at around 1660 MeV. In fact this possibility is remote, since the $Y^*(1660) \rightarrow \Sigma\pi\pi$ decay is believed to take place via the channel $Y^*(1405)\pi$, and hence the reaction

$$K^-p \rightarrow Y^*(1660)\pi^-$$

cannot populate the $\Sigma^+\pi^0\pi^0\pi^-$ final state.

ticles,³¹ produced either by pions or kaons in the beam, where only the Σ^\pm or Ξ^- is observed to decay. These then have the same topology as the " $\Sigma^\pm + \text{pions}$ " final states. The total number of these events was estimated from the number of fits obtained for these rarer final states in the topologies where more than one decay was observed; a suitable correction was applied to allow for the relevant decay modes of the various strange particles. These numbers are shown in the last column of Table V. Of course, it is to be expected that only a small fraction of these will actually fit the hypotheses of interest, especially when there are no missing neutral particles at the production vertex.

It may also be mentioned that, except for the final state $\Sigma^-\pi^+$ in which there are too few events to make a meaningful comparison, the observed χ^2 distributions for the unique events of the different hypotheses are consistent with the expected distributions for the relevant number of constraints.

2. Events Involving Λ^0 and Σ^0

A total of 457 events with two charged pions and a visible Λ decay had kinematic fits to the $K^-p \rightarrow \Lambda^0\pi^+\pi^-$ and $K^-p \rightarrow \Sigma^0\pi^+\pi^-$ hypotheses; about 40% of the events had fits with greater than 5% probability to both of the hypotheses. A small percentage of the events also fitted the $K^-p \rightarrow \Lambda\pi^+\pi^-\pi^0$ hypotheses. It was not possible from a study of the χ^2 alone to decide on selection criteria which would provide fairly pure samples of events in either of the channels.

³¹ The relevant final states for the 2-prong Σ 's are Ξ^-K^+ , $\Xi^-K^+\pi^0$, $\Xi^-K^0\pi^+$, $\Sigma^+K^-K^0$, $\Sigma^-K^+K^0$ produced in K^-p reactions; and $\Sigma^-K^0\pi^+$, $\Sigma^+K^0\pi^-$, $\Xi^-K^+K^0$ produced in π^-p reactions. For 4-prong Σ 's, the only important final states are $\Xi^-K^+\pi^-\pi^+$, $\Xi^-K^+\pi^-\pi^0$ and $\Xi^-K^0\pi^+\pi^-\pi^-$. Unfortunately, the cross section for the reaction $K^-p \rightarrow \Omega^-K^+K^0$ is not large enough for it to be considered as a serious source of contamination.

To get a better idea of the nature of these events, the measured track variables were used to calculate the square of the over-all missing mass and the missing momentum, as well as the errors on these quantities. Events were selected as candidates for the $\Lambda^0\pi^+\pi^-$ and $\Sigma^0\pi^+\pi^-$ hypotheses if the missing mass squared was within 0.01 $(\text{GeV}/c^2)^2$ of zero, the missing momentum within 200 MeV/c of zero, and if the error on the missing mass squared was less than 0.01 $(\text{GeV}/c^2)^2$. Any Σ^0 events giving rise to photons with momenta greater than 200 MeV/c were not resolvable from the low-momentum π^0 background (caused by the $\Lambda\pi^+\pi^-\pi^0$ events) because of the large missing-mass errors. However, the shape of the missing-momentum distribution indicated that the number of such Σ^0 events was less than 10%.

For each of the events in the sample, the mass of the system recoiling against the $\pi^+\pi^-$ pair was computed. A plot of this quantity for the 231 events with missing momentum less than 40 MeV/c exhibited a symmetric peak centered at 1.115 GeV/c². The corresponding plot for the 143 events with missing momentum greater than 70 MeV/c showed a slightly asymmetric peak centered at about 1.2 GeV/c². The 51 events with missing momenta between 40 and 70 MeV/c were found to be extremely ambiguous between $\Sigma^0\pi^+\pi^-$ and $\Lambda^0\pi^+\pi^-$, i.e., most of the events had fitted both hypotheses with fairly high probabilities. These events have been excluded from the effective-mass distributions presented in this paper. This method of selection produces no significant bias in the $\Lambda^0\pi^+\pi^-$ channel, but does tend to remove preferentially the $\Sigma^0\pi^+\pi^-$ events involving Σ^0 's which are highly energetic in the laboratory frame of reference.

A detailed investigation of the pion contamination in the beam led to the conclusion that no significant bias could be introduced by pion-induced strange-particle events.